OXFORD JOURNAL
OF STUDENT
SCHOLARSHIP

Design and Prototyping of a Passive Spinal Brace with Modeled Nonlinear Resistance

Yeonsu Ahn
yeonsuahn0221@gmail.com

ABSTRACT

Passive spinal braces may be designed to distribute resistance differently across a movement interval. However, explicit mechanical comparisons may be required for such concepts. In this study, documented development of EMMA v1 was combined with mathematical analysis of a proposed nonlinear torque profile. A posterior core, lateral panels, and elastic ribs were incorporated by this prototype and fabricated using additive manufacturing. A linear-plus-quadratic model was compared with linear profiles that were matched either for initial stiffness or for terminal torque. Evaluating three illustrative nonlinear parameter settings over 0 - 30°, a transition was assumed at 10°. Relative to linear profiles matched at 30°, the nonlinear profiles reduced initial stiffness by 40.0%, 57.1%, and 72.7% and loading work by 22.2%, 31.7%, and 40.4%, respectively. Greater terminal resistance was provided by nonlinear models against profiles matched for initial stiffness, requiring more work. During prototype development, hinge-tab thickness increased by 14.3% and rib amplitude decreased by 33.3%; these changes were not validated through instrumented mechanical testing. Conditional tradeoffs were established by the findings within the model providing quantitative benchmarks for evaluating future prototypes. To determine whether the fabricated device can realize these resistance profiles or support postoperative rehabilitation, model calibration and physical testing remain necessary.

Keywords: *Spinal orthosis; passive exoskeleton; nonlinear resistance; additive manufacturing; mathematical modeling; mechanical design.*

INTRODUCTION

Postoperative rehabilitation is a potential future application of passive spinal support, but EMMA v1 has not been assessed for clinical use. Randomized trials by Fujiwara et al. and Ma et al. found no consistent clinical or radiographic advantage from routine postoperative bracing in their study populations, although lumbar orthoses are frequently prescribed after fusion (Fujiwara et al., 2019; Ma et al., 2021). Caution was also required for rehabilitation timing. According to Oestergaard et al., poorer outcomes were reported when their rehabilitation program began six rather than twelve weeks after fusion (Oestergaard et al., 2012). These findings support evaluating particular mechanical objectives instead of assuming that recovery is necessarily improved by greater immobilization or earlier movement.

Trunk neuromuscular behavior may be altered by orthoses. Reduced muscle activity was observed by Cholewicki et al. during an unstable sitting task (Cholewicki et al., 2007). However, no detrimental

neuromuscular changes were found by subsequent research after healthy participants wore an orthosis three hours daily for three weeks (Cholewicki et al., 2010). Immediate changes were distinguished by these findings in muscle activation from potential longer-term functional consequences. Back muscle loading has also been reduced by passive elastic garments during leaning and lifting (Lamers et al., 2018), while fatigue was reduced by an elastic exosuit during sustained leaning (Lamers et al., 2020). Mechanical assistance properties were established by these studies, although postoperative safety was not established by their findings.

Methods for translating these principles into modular structures were offered by additive manufacturing. Lin et al. reported comparable clinical outcomes between printed and conventional scoliosis orthoses (Lin et al., 2022). A digital fabrication workflow was demonstrated by Storm et al., evaluating postural stability with printed spinal braces (Storm et al., 2022). Both studies dealt with spinal deformity management, leaving their relevance to postoperative movement control uncertain. Manufacturing considerations were also required by material selection. According to Dolzyk and Jung, printing orientation was shown to influence the tensile and fatigue behavior of polyethylene terephthalate glycol (PETG) (Dolzyk & Jung, 2019). Accordingly, the performance of an assembled brace could not be established by nominal material properties.

Additional design possibilities were provided by architected materials. Schoen described periodic minimal surfaces, including the gyroid, that underpin interconnected lattice geometries (Schoen, 1970). Maskery et al. indicated relationships between lattice topology and deformation mechanisms (Maskery et al., 2018), while polymeric gyroid structures were experimentally and computationally characterized by Abueidda et al. across relative densities (Abueidda et al., 2019). A framework was provided by hyperelastic theory for describing large elastic deformations (Ogden, 1972). Geometry-dependent stiffness and energy absorption were demonstrated by experiments on printed thermoplastic polyurethane structures (Kumar et al., 2022). Together, these findings motivate combining structural geometry with distinct material functions.

In this study, EMMA v1 was examined as a passive brace concept combining a posterior support core, lateral panels, and S-shaped elastic ribs. Its contribution is a comparative analysis of an intended nonlinear resistance profile that was illustrated by documented prototype development. Comparing the model with linear profiles, the model was matched either for initial stiffness or for resistance at the terminal angle. With these comparisons, mathematical design implications were distinguished from unmeasured prototype behavior. With comparisons, resistance redistribution was quantified across the prescribed interval. The research question is about how a thresholded nonlinear resistance model changes initial stiffness and loading work relative to a linear model matched for terminal torque. This study hypothesizes that the nonlinear model will have lower initial stiffness, while requiring less angular work with preserved terminal resistance. This hypothesis concerns model behavior; physical testing is required to determine whether the fabricated ribs reproduce the predicted resistance profile. All angular limits were assumed engineering targets.

METHODS AND MATERIALS

In this study, documented prototype development was combined with deterministic analysis of a proposed resistance profile. Manufacturing information and qualitative observations were extracted from the original design manuscript. From those observations, all model comparisons reported here were separately calculated. The model was not calibrated against measured torque. In addition, no human participants, patient records, or clinical outcomes were included in the analysis.

The modular brace consisted of a posterior core, two lateral panels, and four elastic ribs. The nominal core had a height of 420mm, widths of 60, 80, and 100mm at its upper, middle, and lower regions and thickness of 4.5mm. Each panel had 130mm height and 2.5mm thickness. Rib dimensions were 300 x 15 x 3 mm. Components were designed in Fusion 360 and exported as STL files. Polyamide 12 was the intended core material. PETG was used for the documented prototype for both core and panels and thermoplastic polyurethane, TPU 95A, for the ribs.

A printer with a 220 x 220 x 250 mm build volume was used for fabrication. A 240°C nozzle, 75°C bed, 0.2mm layers, and 40% gyroid infill were used to print the PETG components. For TPU ribs, a 225°C nozzle, 0.2mm layers, 100% infill, and printing speed of 20mm/s were used. The core was divided into two nominally 220mm sections with 20mm overlap, and joined using screws and epoxy. Hinge-tab thickness and rib amplitude were the focus of documented revisions. Without attributing measured mechanical benefits, these changes were treated as fabrication observations.

Resistance was represented by the following phenomenological model, where M is torque magnitude, θ is device bending angle in degrees, and θc is the assumed onset of increasing stiffness.

$M(\theta) = k_0\theta + k_1[\max(0, \theta-\theta c)]^2,\ 0 \leq \theta \leq 30°$

Here, k0 has units of newton meters per degree and k1 has units of newton meters per degree squared. Both coefficients were positive. In the analysis, θc = 10° and a terminal angle of 30° were used. These values place the transition at one-third of the modeled interval, allowing a simple normalized comparison over $0 \leq x \leq 3$. They are illustrative engineering choices, not clinically validated movement limits. Engineering scenarios were defined by these values without specifying permissible spinal movement. Since behavior beyond the terminal angle was outside this mathematical analysis, the proposed mechanical stop was excluded. Normalizing the angle by θc and torque by M(θc) yields the dimensionless representation below. Λ represents nonlinear resistance relative to initial stiffness.

$$x = \frac{\theta}{\theta c},\ \lambda = \frac{k1\theta c}{k0},\ mN(x) = \frac{M(\theta)}{M(\theta c)} = x + \lambda[(0,\ x - 1)\ ]^2$$

Three illustrative values of λ were examined as 0.5, 1, and 2. These values provide a compact sensitivity comparison by halving and doubling the nonlinear contribution relative to the reference scenario λ = 1. They do not represent clinically validated resistance targets. After constructing two linear comparators, one matched the nonlinear models' initial stiffness. The other matched its torque at 30°.

$$mI(x) = x,\ mT(x) = \left(1 + \frac{4\lambda}{3}\right)x$$

Normalized torque, initial stiffness, and the mechanical work required for monotonic loading from 0° to 30° were evaluated by comparisons. Work was calculated by integrating torque with respect to angle, converting degrees to radians before interpreting dimensional energy.

$$w = \int_0^3 m(x)dx,\ W = \frac{\pi\theta c}{180}M(\theta c)w$$

Stiffness and work reductions were calculated relative to the linear comparator matched at 30°, deriving and checking the closed expressions against numerical integration. Loading work was denoted by mechanical work without energy dissipation, physiological effort, or patient benefit. The analysis assumed quasistatic loading and omitted hysteresis, friction, deformation of other components, and interactions with the body. As the scenarios were deterministic without available experimental replicates, no inferential statistical tests were applied. Prototype observations and theoretical findings were separately reported throughout.

RESULTS

In the documented prototype, a PETG posterior core and lateral panels were combined with four TPU ribs. From the intended PA12 core design, its material configuration differed. The 420mm core exceeded the printer's 250mm vertical capacity by 170mm, or 68.0%, and was assembled from two overlapping sections. There was an increase in hinge-tab thickness from 3.5 to 4.0mm, a 14.3% increase, while there was a decrease observed in rib amplitude from ±12 to ±8mm, a 33.3% reduction in magnitude. These nominal design revisions were summarized in Figure 1. Reported improvements in fit and perceived resistance were not used to estimate model coefficients as they remained qualitative. Therefore, changes in hinge-tab thickness and rib amplitude cannot yet be interpreted as producing the modeled nonlinear resistance profile.

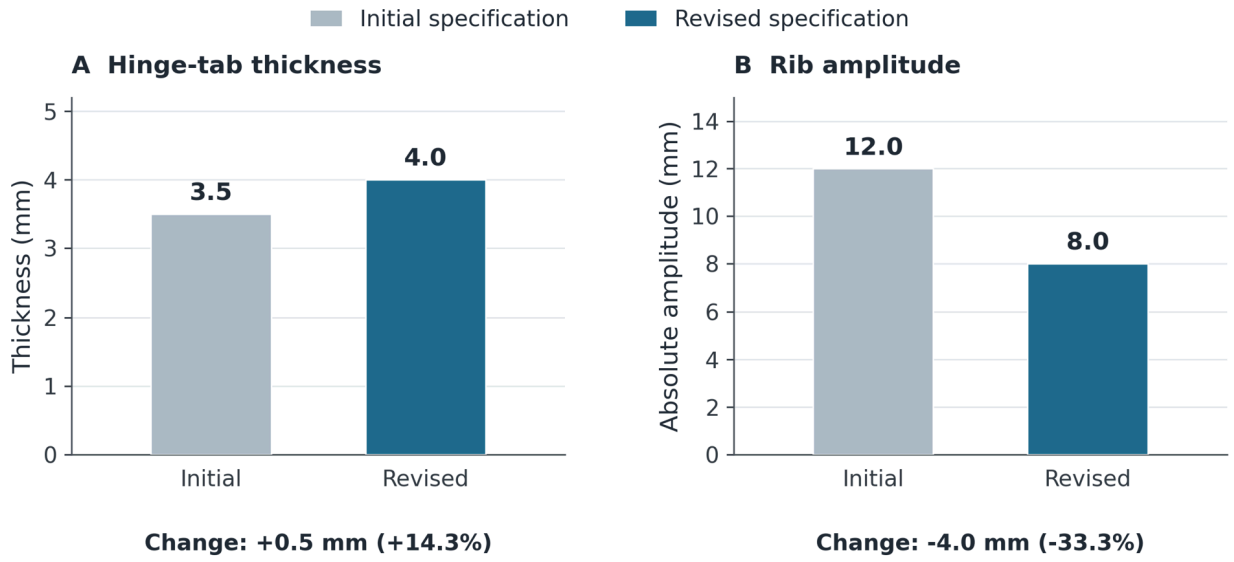


Figure 1. Prototype Design Revisions. Changes in nominal hinge-tab thickness and rib amplitude during prototype development; these dimensions do not quantify changes in mechanical performance.

Identical torque of 1 at 10° was produced by the normalized nonlinear model for all three parameter settings. At 20°, torque was 2.5, 3.0, and 4.0 for λ values of 0.5, 1, and 2, respectively. Corresponding torque at 30° was 5.0, 7.0, and 11.0, as reported in Table 1. The linear model matched for initial stiffness produced torque of 3.0 at 30°. Therefore, terminal torque increased in the nonlinear scenarios by 66.7%, 133.3%, and 266.7% relative to that comparator while the same modeled response from 0° through 10° was preserved.

Assumed λ	**Normalized torque at 20°**	**Normalized torque at 30°**	**Initial stiffness reduction (%)**	**Loading work reduction (%)**
0.5	2.5	5.0	40.0	22.2
1.0	3.0	7.0	57.1	31.7
2.0	4.0	11.0	72.7	40.4

Table 1. Calculated resistance and work comparisons for three illustrative nonlinear parameter settings. Torque was normalized by nonlinear torque at 10°. Reductions were relative to a linear profile matched to each scenario's torque at 30°. All values are calculated model outputs.

Normalized linear stiffness of 1.667, 2.333, and 3.667 was produced by matching the linear comparator to each nonlinear scenario's torque at 30°. Each nonlinear model had initial stiffness of 1. Consequently, initial stiffness was lower by 40.0%, 57.1%, and 72.7%, respectively. For the middle scenario, nonlinear and terminally matched linear torque both reached 7.0 at 30°. However, torque at 10° was 1.0 versus

2.333. In Figure 2, this comparison was illustrated alongside the initial-stiffness comparator. Algebraically, throughout the open interval between 0° and 30°, nonlinear torque remained below the terminally matched linear profile with equality at both endpoints. There was an increase observed in incremental stiffness across the modeled interval. For λ = 1, its normalized value increased from 1 at 10° to 5 at 30° without a discontinuity in either torque or stiffness.

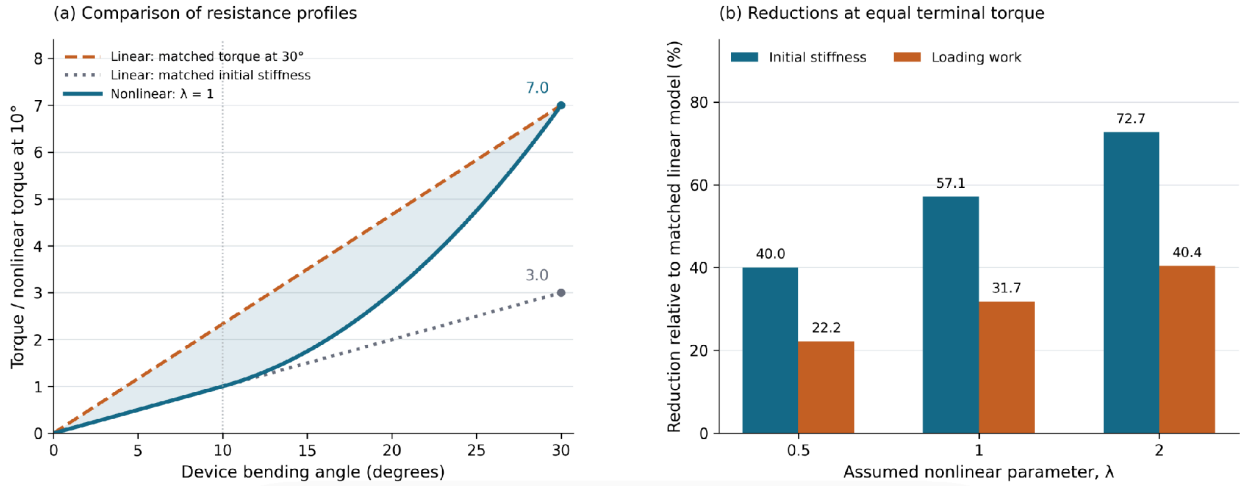


Figure 2. (a) Nonlinear resistance at λ = 1 compared with linear profiles matched for initial stiffness or terminal torque. Shading represents the difference in loading work from the terminally matched comparator. (b) Calculated stiffness and work reductions for three parameter settings.

Normalized loading work for the nonlinear scenarios was 5.833, 7.167, and 9.833, compared with 7.500, 10.500, and 16.500 for their terminally matched linear counterparts. These values show the dimensionless area under each torque curve. Relative work reductions were observed to be 22.2%, 31.7%, and 40.4% respectively. The percentage reduction in work equaled five ninths of the percentage reduction in initial stiffness for a fixed transition at one third of the terminal angle. This relationship held for every positive λ within the specified model instead of only for the three illustrated scenarios.

$$wN = \frac{9}{2} + \frac{8\lambda}{3},\ wT = \frac{9}{2} + 6\lambda$$

$$1 - \frac{wN}{wT} = \frac{20\lambda}{27+36\lambda} = \frac{5}{9}\left(1 - \frac{1}{1+4\lambda/3}\right)$$

The stated study hypothesis was supported by the comparisons within the mathematical framework: terminal resistance could be preserved while initial stiffness and loading work were reduced relative to a linear profile. Less work was required by the linear comparator matched for initial stiffness, but lower terminal resistance was provided. This demonstrated that the chosen matching condition affected the conclusions. A conditional tradeoff between resistance distribution and loading work has been established by these results. The analysis did not identify which λ described the printed ribs or establish their absolute

torque capacity. For joint integrity, cyclic durability, contact pressure, breathing accommodation, or muscle activation, no measurements were available. No clinical performance outcomes were inferred.

DISCUSSION

The mathematical objective of EMMA v1 was clarified in the analysis. The nonlinear profile was allowed by the matching terminal torque to reduce initial stiffness and loading work at the same time. With this result, the proposed redistribution of resistance was quantified to larger angles, providing a benchmark for evaluating future prototypes. However, it does not establish that the fabricated ribs reproduce the assumed profile.

Interpretation was materially changed by the comparator selection. Against a linear model with the same initial stiffness, greater terminal resistance was provided by the nonlinear profile, requiring more loading work. Against a linear model with the same terminal resistance, it requires less work. Accordingly, reduced loading work should always be reported with its matching condition. Therefore, it cannot be directly interpreted as reduced muscular effort or improved rehabilitation. It is still an unresolved design decision about how to select a clinically appropriate resistance target.

This distinction is relevant to trials that found limited benefits from routine postoperative bracing (Fujiwara et al., 2019; Ma et al., 2021). According to passive exosuit studies, assistance may alter muscular loading without validating clinical effects of EMMA (Lamers et al., 2018; Lamers et al., 2020).

The analysis in this study has several limitations. First, the model coefficients were assumed, and the relationship between λ and rib geometry, printing conditions, or material properties was not established. Second, hysteresis, friction, and interactions between brace components and the body were omitted in quasistatic calculations. The intended PA12 core was replaced by PETG, while additional structural uncertainty was introduced by assembly joints. The next validation step is bench torque-angle testing of the assembled prototype, followed by model calibration and comparison with independent loading trials. Whether the modeled tradeoffs can guide further development of the physical design may then be determined by durability and interface measurements.

CONCLUSION

In this study, documented development of EMMA v1 was combined with a comparative mathematical analysis of its intended resistance profile. How increasing resistance beyond an assumed transition angle could preserve terminal torque was shown in the model while reducing initial stiffness and loading work relative to a matched linear profile. Initial stiffness decreased by 40.0 – 72.7% and loading work by 22.2 – 40.4% across three illustrative parameter settings. A conditional design tradeoff was quantified by these results, while supplying comparison targets for future testing. The prototype contributed manufacturing observations, including revisions to hinge-tab thickness and rib amplitude. However, the modeled mechanical response was not established. Therefore, a reproducible comparison framework linked to a documented brace concept was the principal contribution. Experimental calibration was still needed to connect the mathematical parameters with actual rib geometry and material behavior. Repeatability,

durability, and interface performance should be established by subsequent evaluation before considering clinical applications. Postoperative rehabilitation remains a potential future application requiring separate evaluation of safety and effectiveness after mechanical validation.

REFERENCES

Abueidda, D. W., Elhebeary, M., Shiang, C. S., Pang, S., Abu Al-Rub, R. K., & Jasiuk, I. M. (2019). Mechanical properties of 3D printed polymeric Gyroid cellular structures: Experimental and finite element study. Materials & Design, 165, Article 107597. https://doi.org/10.1016/j.matdes.2019.107597

Cholewicki, J., McGill, K. C., Shah, K. R., & Lee, A. S. (2010). The effects of a three-week use of lumbosacral orthoses on trunk muscle activity and on the muscular response to trunk perturbations. BMC Musculoskeletal Disorders, 11, Article 154. https://doi.org/10.1186/1471-2474-11-154

Cholewicki, J., Reeves, N. P., Everding, V. Q., & Morrisette, D. C. (2007). Lumbosacral orthoses reduce trunk muscle activity in a postural control task. Journal of Biomechanics, 40(8), 1731–1736. https://doi.org/10.1016/j.jbiomech.2006.08.005

Dolzyk, G., & Jung, S. (2019). Tensile and fatigue analysis of 3D-printed polyethylene terephthalate glycol. Journal of Failure Analysis and Prevention, 19, 511–518. https://doi.org/10.1007/s11668-019-00631-z

Fujiwara, H., Makino, T., Yonenobu, K., Moriguchi, Y., Oda, T., & Kaito, T. (2019). Efficacy of lumbar orthoses after posterior lumbar interbody fusion—a prospective randomized study. Medicine, 98(15), Article e15183. https://doi.org/10.1097/MD.0000000000015183

Kumar, A., Collini, L., Ursini, C., & Jeng, J.-Y. (2022). Energy absorption and stiffness of thin and thick-walled closed-cell 3D-printed structures fabricated from a hyperelastic soft polymer. Materials, 15(7), Article 2441. https://doi.org/10.3390/ma15072441

Lamers, E. P., Soltys, J. C., Scherpereel, K. L., Yang, A. J., & Zelik, K. E. (2020). Low-profile elastic exosuit reduces back muscle fatigue. Scientific Reports, 10, Article 15958. https://doi.org/10.1038/s41598-020-72531-4

Lamers, E. P., Yang, A. J., & Zelik, K. E. (2018). Feasibility of a biomechanically-assistive garment to reduce low back loading during leaning and lifting. IEEE Transactions on Biomedical Engineering, 65(8), 1674–1680. https://doi.org/10.1109/TBME.2017.2761455

Lin, Y., Cheung, J. P. Y., Chan, C. K., Wong, S. W. F., Cheung, K. M. C., Wong, M., Wong, W. C., Cheung, P. W. H., & Wong, M. S. (2022). A randomized controlled trial to evaluate the clinical effectiveness of 3D-printed orthosis in the management of adolescent idiopathic scoliosis. Spine, 47(1), 13–20. https://doi.org/10.1097/BRS.0000000000004202

Ma, H.-H., Wu, P.-H., Yao, Y.-C., Chou, P.-H., Lin, H.-H., Wang, S.-T., & Chang, M.-C. (2021). Postoperative spinal orthosis may not be necessary for minimally invasive lumbar spine fusion surgery: A prospective randomized controlled trial. BMC Musculoskeletal Disorders, 22, Article 619. https://doi.org/10.1186/s12891-021-04490-4

Maskery, I., Sturm, L., Aremu, A. O., Panesar, A., Williams, C. B., Tuck, C. J., Wildman, R. D., Ashcroft, I. A., & Hague, R. J. M. (2018). Insights into the mechanical properties of several triply periodic minimal surface lattice structures made by polymer additive manufacturing. Polymer, 152, 62–71. https://doi.org/10.1016/j.polymer.2017.11.049

Oestergaard, L. G., Nielsen, C. V., Bünger, C. E., Søgaard, R., Fruensgaard, S., Helmig, P., & Christensen, F. B. (2012). The effect of early initiation of rehabilitation after lumbar spinal fusion: A randomized clinical study. Spine, 37(21), 1803–1809. https://doi.org/10.1097/BRS.0b013e31825a17ab

Ogden, R. W. (1972). Large deformation isotropic elasticity—On the correlation of theory and experiment for incompressible rubberlike solids. Proceedings of the Royal Society of London. Series A, Mathematical and Physical Sciences, 326(1567), 565–584. https://doi.org/10.1098/rspa.1972.0026

Schoen, A. H. (1970). Infinite periodic minimal surfaces without self-intersections (NASA Technical Note D-5541). National Aeronautics and Space Administration. https://ntrs.nasa.gov/citations/19700020472

Storm, F. A., Redaelli, D. F., Biffi, E., Reni, G., & Fraschini, P. (2022). Additive manufacturing of spinal braces: Evaluation of production process and postural stability in patients with scoliosis. Materials, 15(18), Article 6221. https://doi.org/10.3390/ma15186221